Adsorbed-Iodine-Catalyzed Dissolution of Pd Single-Crystal Electrodes: Studies by Electrochemical Scanning Tunneling Microscopy

ARTICLE *in* THE JOURNAL OF PHYSICAL CHEMISTRY · DECEMBER 1996

Impact Factor: 2.78 · DOI: 10.1021/jp9620532

3 AUTHORS, INCLUDING:

Kingo Itaya
Tohoku University
246 PUBLICATIONS **8,355** CITATIONS

SEE PROFILE

Adsorbed-Iodine-Catalyzed Dissolution of Pd Single-Crystal Electrodes: Studies by Electrochemical Scanning Tunneling Microscopy

K. Sashikata,[†] Y. Matsui,[†] and K. Itaya*,[†]

Itaya Electrochemiscopy Project, ERATO/JRDC, 2-1-1 Yagiyama-minami, Taihaku-ku 982 Japan

M. P. Soriaga*

Department of Chemistry, Texas A&M University, College Station, Texas 77843

Received: July 10, 1996; In Final Form: September 16, 1996[⊗]

Unfettered anodic dissolution occurs in *halide-free* sulfuric acid solutions for Pd electrodes pretreated with a single chemisorbed layer of iodine atoms; no dissolution takes place in the absence of iodine. Tandem cyclic voltammetry and in situ scanning tunneling microscopy have been employed to investigate the mechanism of this type of corrosion *under low-current conditions*. The ordered adlattices studied were those spontaneously formed upon immersion of the Pd single-crystal surface to a dilute solution of iodide: Pd(111)-($\sqrt{3} \times \sqrt{3}$)-*R*30°-I; Pd(100)-*c*(2 × 2)-I; Pd(110)-pseudohexagonal-I. It has been found that (i) adsorbed-iodine-catalyzed corrosion of Pd is a structure-sensitive reaction; it decreases in the order Pd(110)−I > Pd(111)−I ≥ Pd(100)−I. (ii) At Pd(111)−I, dissolution occurs exclusively at step-edges in a layer-by-layer sequence without deterioration of the iodine adlattice structure. (iii) At Pd(100)−I, dissolution takes place anisotropically along a step aligned in the {100} direction but in a layer-by-layer process without disruption of the iodine adlattice structure. (iv) At Pd(110)−I, dissolution transpires predominantly at a step-edge that runs parallel to the {100} direction; pit formation at terraces precluded layer-by-layer dissolution and led to progressive disorder of the substrate structure. Heuristic models are presented to account for these observations.

Introduction

The need to document and rationalize, at the atomic level, relationships between surface structure, surface composition, and surface reactivity cannot be overemphasized. The application of powerful, surface-sensitive analytical methods based upon electron and ion spectroscopies has led to dramatic advances in the study of gas−solid[1] and liquid−solid[2] interfaces. Such techniques, however, need to be carried out in a rarefied environment and, in the realm of reactivity studies, can specify only initial-state (prior to immersion) and final-state (after emersion) features; information, in the course and under the conditions of a given reaction, can only be inferred indirectly.

A host of surface analytical methods, collectively dubbed as in situ techniques, have recently been developed[3] to permit (albeit not without difficulty) measurements entirely under electrochemical conditions; one of these techniques is scanning tunneling microscopy, STM.[4] The combination of electrochemistry with STM (EC−STM) has paved the way for the recent resurgence in research in electrochemical surface science.[5,6] A more complete strategy may be afforded by the integration of EC−STM with other analytical methods that make possible the determination of surface composition, thermodynamics, electronic structure, and chemical bonding; the combination of EC−STM with ultrahigh vacuum (UHV) techniques serves as one example of such a scheme.[7,8]

In this paper, we present results based upon EC−STM that extend the detail of information known about adsorbate-catalyzed anodic dissolution, a relatively under-studied interfacial phenomenon, in which the corrosion of a metal substrate is induced by a single monolayer of certain adsorbates in a solution devoid of corrosion promoters.[9−12]

The case under scrutiny is the dissolution of Pd single-crystal electrodes in *halide-free* sulfuric acid solutions catalyzed by a single adsorbed layer of zero-valent iodine atoms.[10−12] Initial structural work, based upon tandem UHV spectroscopy [low-energy electron diffraction (LEED) and Auger electron spectroscopy (AES)] and electrochemistry of oriented Pd bulk single crystals, revealed that (i) the structure and composition of the iodine adlattices formed at Pd(111)[10] and Pd(100)[11] were preserved even after prolonged dissolution and (ii) progressive disorder of the Pd(110)−I[12] interface is brought about by the dissolution reaction despite the fact that the iodine coverage is unaltered. Ordered layer-by-layer dissolution is indicated at Pd(100) and Pd(111) but not at Pd(110). Beyond these pre- and postcorrosion structural and compositional information, little else can be gleaned directly from the UHV−EC approach. The mode of dissolution, for example, cannot be unambiguously ascertained. It is on this particular issue that the present EC−STM work has been focused.

Experimental Section

Single-crystal surfaces of palladium were prepared by the Clavilier method.[13] A Pd wire of 99.995% purity was melted in an oxygen-rich hydrogen flame and slowly cooled to obtain, at the end of the wire, a single-crystal bead 3 mm in diameter. Eight facets (0.2 mm in diameter), oriented in the (111) plane, and six smaller facets (0.08 mm in diameter), oriented in the (100) plane, appeared on the single-crystal bead in octahedral and hexagonal arrangements, respectively. From geometric considerations of a face-centered cubic lattice, the (110) plane was deduced from the positions of the (111) and (100) facets. To enable electrochemical measurements, which necessitated larger surface areas larger than even the (111) facet, the beads were metallographically polished along the desired orientations; crystallographic alignment was by laser-spot reflection. Damaged selvage layers were removed by annealing at 1000 °C for

[†] Department of Applied Chemistry, Faculty of Engineering, Tohoku University, Sendai 980, Japan.

* To whom correspondence should be addressed.

[⊗] Abstract published in *Advance ACS Abstracts,* November 1, 1996.

S0022-3654(96)02053-9 CCC: $12.00

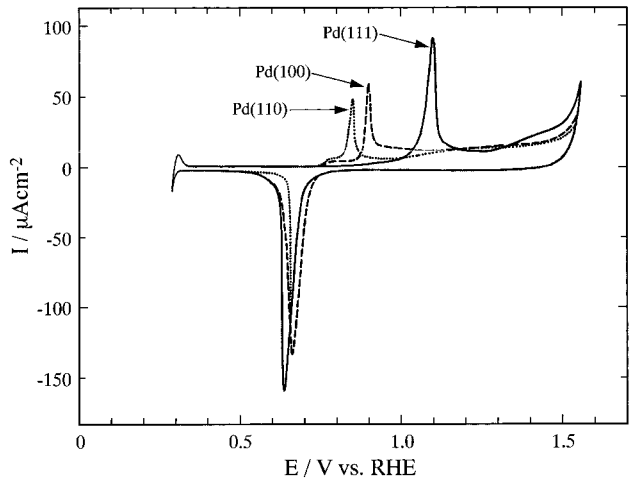

Figure 1. Cyclic voltammograms obtained at iodine-free Pd(111), Pd(100), and Pd(110) single-crystal electrodes in 0.05 M H_2SO_4. The potential scan rate was 20 mV/s.

ca. 2 h. Final treatment of the clean and ordered surfaces consisted of flame annealing, slow cooling (in a stream of high-purity inert gas), and immersion in ultrapure water (to prevent environmental contamination).

Iodine pretreatment was accomplished simply by immersion of the clean electrode, without potential control, in an aqueous 1 mM solution of iodide for 5 min. Unadsorbed iodide was removed by rinsing with pure water. All solutions were prepared from H_2SO_4 (Merck, Suprapure grade), KI (Merck, Suprapure grade), and Milli-Q Plus water (Millipore Systems). Potentials were referenced against the reversible hydrogen electrode (RHE).

In situ STM was carried out with either a Seiko SP-3700 (Seiko Instruments) or Nanoscope II (Digital Instruments) instrument equipped with a custom-built Kel-F electrochemical cell. The STM probe was a Pt wire imbedded in a glass capillary in such a manner that only the tip-point was exposed; Faradaic currents were minimized in this configuration. The residual background current of the STM tip at a potential in the double layer region was less than 20 pA. Experimental details have been presented elsewhere.[14]

Results and Discussion

Electrochemistry. Based upon earlier studies with the more widely used noble-metal electrodes,[13,15] the electrochemistry of *iodine-free* palladium was expected to be dependent upon the crystallographic orientation of the surface in contact with the electrolyte. This expectation was borne out by the data in terms of cyclic voltammograms of Pd(111), Pd(100), and Pd(110) in 0.05 M H_2SO_4, shown in Figure 1. All three single-crystal surfaces exhibited sharp anodic oxidation peaks at potentials E_{ox} that increased in the following order: Pd(110) (E_{ox} = 0.85 V) < Pd(100) (E_{ox} = 0.90 V) < Pd(111) (E_{ox} = 1.10 V). In contrast, only a broad, undefined peak can be obtained at a polycrystalline surface.[10]

The E_{ox} data indicate that the propensity for surface-oxide formation, thought to occur stepwise as follows[16]

$$Pd + H_2O \rightarrow Pd{-}OH_{(s)} + H^+ + e^- \quad (1)$$

$$Pd{-}OH_{(s)} \rightarrow PdO_{(s)} + H^+ + e^- \quad (2)$$

is greatest at Pd(110) and least at Pd(111). The structure-sensitivity of E_{ox} almost certainly originates from differences in surface−atom arrangements at the three low-index planes. For a face-centered cubic lattice, the number of nearest-neighbors (coordination number) for an atom on the (111) surface is 9; those for atoms on the (100) and (110) planes are 8 and 7, respectively. Since the reactivity of a surface atom generally decreases as its coordination number increases,[1,15a,15b,17] the greater reactivity of the (110) plane relative to the (111) plane is not unexpected.

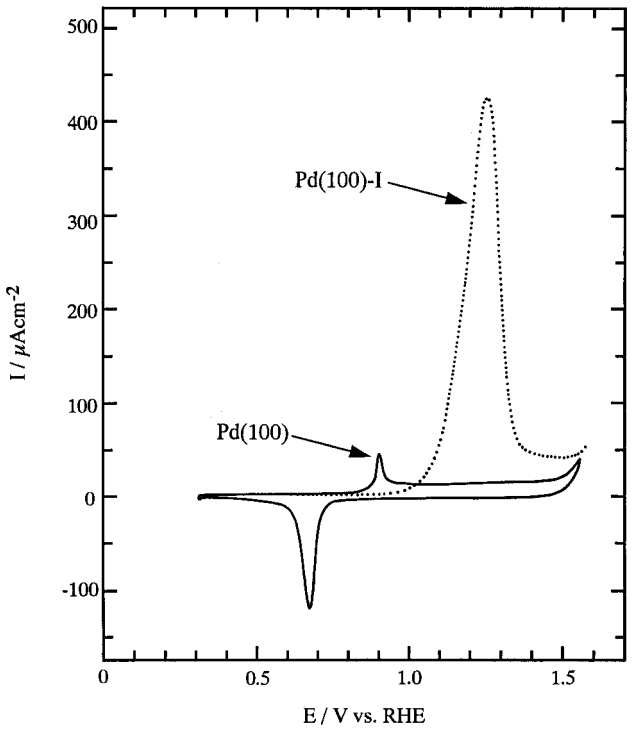

Figure 2. Cyclic voltammograms of I-free and I-pretreated Pd(100) single-crystal electrode in 0.05 M H_2SO_4. The potential scan rate was 20 mV/s.

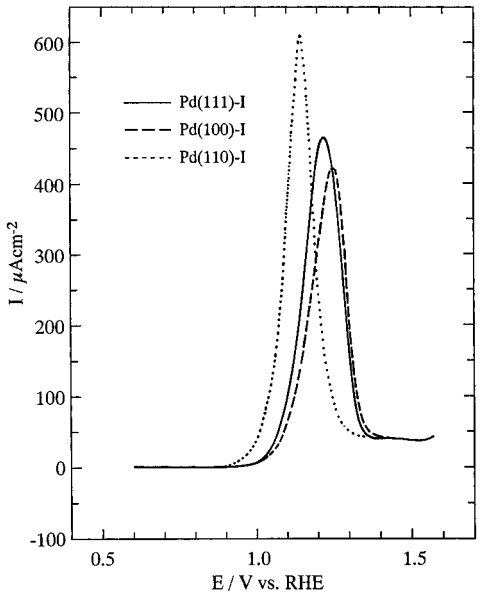

Figure 3. Cyclic voltammograms of I-pretreated Pd(111), Pd(110), and Pd(100) single-crystal electrodes in 0.05 M H_2SO_4. The potential scan rate was 20 mV/s.

It is noteworthy that coulometric curves observed during the surface oxidation of the Pd single-crystal electrodes up to 1.5 V showed the charges of ca. 870, 810, and 600 μC/cm^2 for the (111), (100), and (110) surfaces, respectively. The calculated charges for monlayer oxide formation are 490, 430, and 300 μC/cm^2 for the corresponding ideal (1 × 1) surfaces, respectively, assuming an overall two-electron-transfer reaction (eqs 1 and 2). The experimental values shown above suggest that

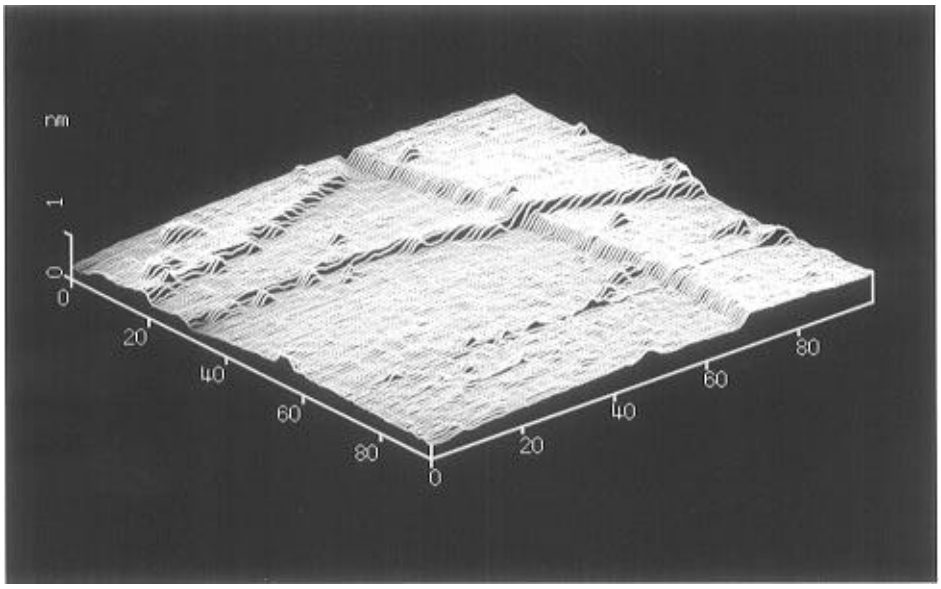

Figure 4. Medium-resolution scanning tunneling microscope image of an iodine-free Pd(111) single-crystal electrode at 0.4 V in 0.05 M H_2SO_4. The potential of the tip was 0.9 V; the tunneling current was 1 nA.

the oxidation of the Pd surfaces occurs in the first two layers. On the other hand, it is well-known that the charges consumed for the oxidation of Pt and Au electrodes up to 1.5 V are in a range of 400−450 μC/cm^2, which corresponds to the oxidation of the first layer of the Pt[6c,18,19] and Au[20] surfaces.

It is important to mention the following. (i) In 0.1 M $HClO_4$, current−potential curves nearly identical with those in Figure 1 were obtained; that is, "butterfly" peaks similar to those for Pt(111)[11] in 0.1 *M* $HClO_4$ were not observed for Pd(111). (ii) The cathodic currents that become appreciable at ca. 0.3 V are due to (reversible) hydrogen *absorption*; the onset potential for this bulk reaction is independent of the surface crystallographic plane.

When the Pd electrodes are pretreated with iodine and cyclic voltammograms, under conditions identical with those in Figure 1, and are reacquired, dramatic alterations take place, as can be seen in Figure 2 for an iodine-coated Pd(100) surface. The two more notable features are (i) the suppression of the surface-oxidation peak at E_{ox} and (ii) the emergence of a new anodic peak (E'_{ox} = 1.25 V) that, at a potential scan rate of 20 mV/s, yields a peak current nearly an order-of-magnitude larger than that for the I-free surface. If the potential is held at a value *just below* E'_{ox}, the current does not decay but remains essentially constant, a behavior diagnostic of a material-limited dissolution process.

One other important effect of iodine pretreatment, although not shown in the voltammetric data in Figure 2, is the retardation by more than −100 mV of the onset-potential for the hydrogen absorption reaction. Note that the hydrogen desorption peak also decreased upon I chemisorption. These results signify that although hydrogen absorption is a structure-insensitive reaction, it is influenced by the surface composition.

Previous studies of polycrystalline and single-crystal Pd electrodes, based upon techniques that included coulometry, atomic emission spectroscopy, electron diffraction, and surface elemental analysis, have established the follwoing.[7−10] (i) The anodic peak is due to the two-electron dissolution reaction

$$Pd_{(s)} \rightarrow Pd^{2+}_{(aq)} + 2e^- \qquad (3)$$

(ii) The rate of corrosion is directly proportional to the fractional coverage of iodine $\theta_I \equiv \Gamma_I/\Gamma_{I,max}$. (iii) The iodine coverages remain constant throughout the dissolution process. (iv) The long-range structures of the iodine adlattices formed at Pd(111)

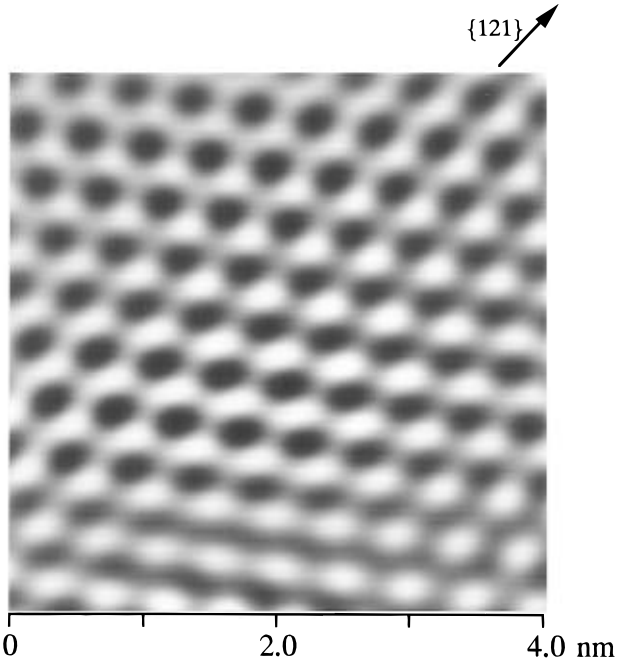

Figure 5. High-resolution STM image of Pd(111)-($\sqrt{3} \times \sqrt{3}$)*R*30°-I at 0.75 V in 0.05 M H_2SO_4. The potential of the tip was 0.9 V; the tunneling current was 1 nA.

and Pd(100) remain well-ordered after the corrosion reaction. (v) In the presence of coadsorbed oxide, such as at potentials more positive than E'_{ox}, the adsorbed iodine is rendered unstable toward oxidative desorption as IO_3^- ions; consequently, the surface becomes oxide-passivated and the dissolution reaction subsides.

Cyclic voltammograms for the dissolution of Pd(111)−I, Pd(100)−I, and Pd(110)−I surfaces in 0.05 M H_2SO_4 are shown in Figure 3. The data demonstrate that the chemisorbed-iodine-catalyzed dissolution of Pd is also a structure-sensitive reaction. The ease by which Pd corrosion transpires decreases in the order Pd(110)−I > Pd(111)−I ≥ Pd(100)−I.

In Situ STM. *(i) Pd(111)−I.* In 0.05 M H_2SO_4 and at potentials within the double-layer region (0.3 V < *E* < 0.7 V), wide atomically flat terraces with monatomic steps that intersected one another at angles of 60° or 120° were observed at both iodine-free (Figure 4) and iodine-pretreated Pd(111). The atomic-resolution image of the I-coated surface, prior to the

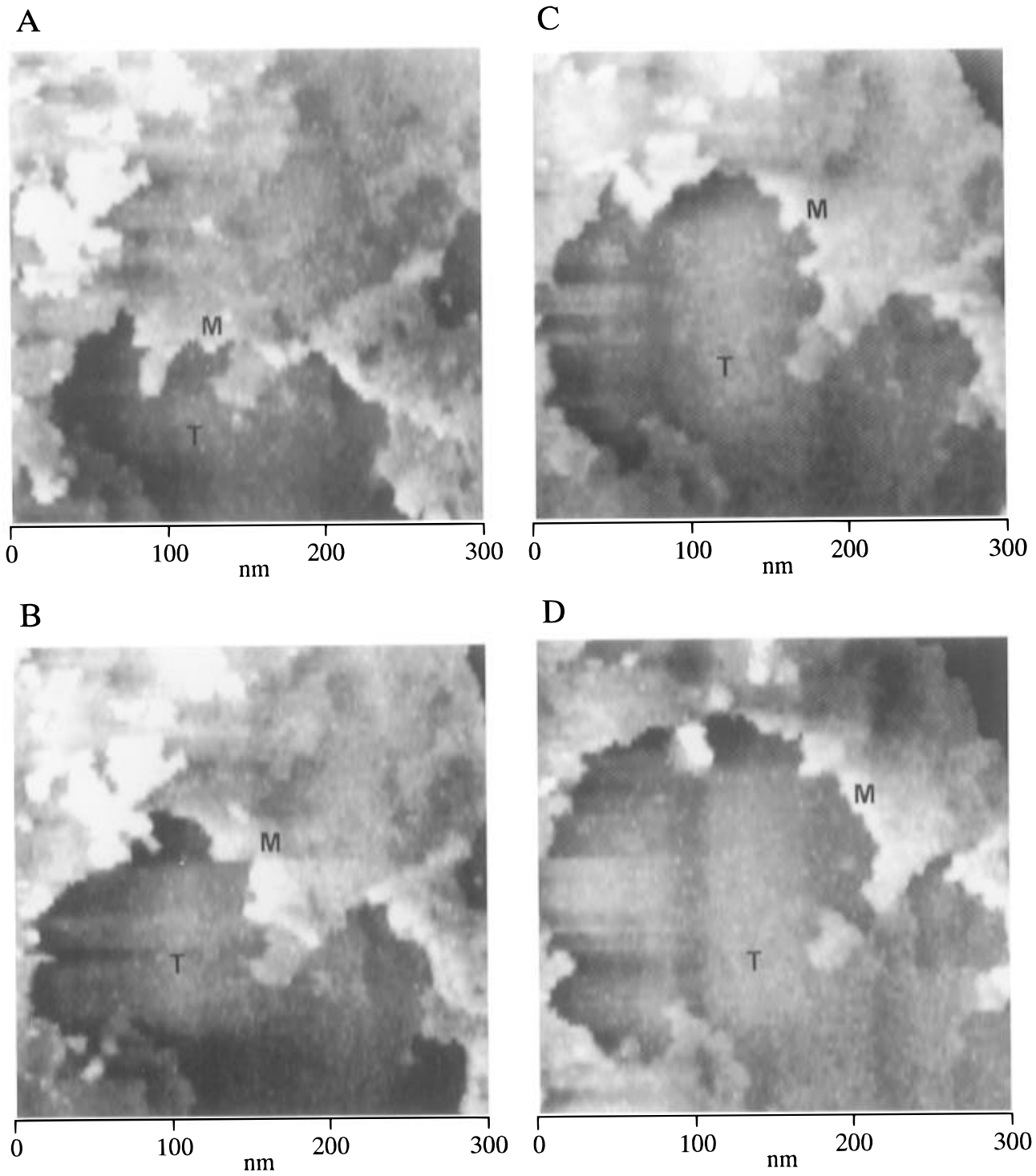

Figure 6. Wide-area STM images of Pd(111)-($\sqrt{3} \times \sqrt{3}$)*R*30°-I at (A) 10, (B) 20, (C) 25, and (D) 30 min after anodic dissolution at 1.05 V in 0.05 M H_2SO_4. The letter T designates a terrace, whereas the letter M denotes a step-edge. The potential of the tip was 0.9 V; the tunneling current was 1 nA.

dissolution experiments, is shown in Figure 5. It will be mentioned that the image shown was obtained after 1 h of equilibration, a condition necessary to attain minimum thermal drift. The iodine adatoms are aligned along the {121} direction, that is, along a vector rotated 30° with respect to the substrate-atom rows. The distance between nearest-neighbor atoms was determined to be 0.47 ± 0.01 nm. The observed structure, Pd(111)-($\sqrt{3} \times \sqrt{3}$)*R*30°-I, is identical with that reported earlier based upon LEED measurements.[10]

After acquisition of the image in Figure 5, the potential was then scanned to and held at 1.05 V, a potential at which metal dissolution is initiated. Figure 6 presents a series of STM images, in the same (300 × 300 nm^2) domain, obtained 10, 20, 25, and 30 min after the start of the anodic dissolution. In this sequence of images, the progress of dissolution can be monitored via topographical changes in the terrace (designated by a T) and the step-edge (marked with an M) within the rastered domain. It is easy to recognize that as the *low-current* dissolution proceeds, (i) the step-edge retracts upward, (ii) the area of the lower terrace increases, and (iii) the (diminished) upper terrace and (enlarged) lower terrace remain pit-free. In addition to these readily obvious features, one can also note (i) the gradual dissolution of the islands on the upper left-hand corner in Figure 6A and (ii) the characteristic jagged outline (contour) of the receding upper terrace. The latter observation

hints at preferential dissolution along either substrate or adsorbate atomic rows.

The images serialized in Figure 6 clearly point to a *step-selective layer-by-layer* dissolution mechanism.

High-resolution STM of the postcorrosion terrace revealed an iodine adlattice structure identical with that shown in Figure 5; that is, a well-ordered Pd(111)-($\sqrt{3} \times \sqrt{3}$)*R*30°-I adlattice was retained after the corrosion reaction. This observation is in consonance with data reported earlier on the basis of UHV−EC measurements.[10]

(ii) Pd(100)−I. As with the Pd(111) surface, atomically flat terraces with monatomic steps were observed at both the clean and iodine-coated Pd(100) facets in 0.05 M H_2SO_4 in the double-layer region. An ordered iodine adlayer structure was also observed at flat terraces, typified by the high-resolution STM image in Figure 7. Owing to thermal drift, a slight distortion of the image may be noted. However, by comparison with the clean-substrate image, it is possible to ascertain that the iodine adatoms are aligned along the {110} direction, 45° with respect to the {100} direction; a nearest-neighbor distance of 0.38 nm was measured. This interfacial configuration is consistent with a Pd(100)-*c*(2 × 2)-I adlattice structure previously determined by LEED experiments.[11]

Dissolution at 0.95 V. Figure 8A shows a wide-area STM image of the Pd(100)-*c*(2 × 2)-I adlattice prior to anodic dissolution. Two types of steps can be seen in this image. One, parallel to the {110} iodine-atom rows, varies in height from one (labeled S'_2) to several (S_2) atomic layers. The other, aligned along the {100} direction, 45° with respect to the {110} direction, is only one atomic layer in height; this step is labeled S_1. No changes were observed with S_1, S'_2, or S_2 at 0.9 V, even after 30 min.

The STM image of the Pd(100)-*c*(2 × 2)-I adlattice obtained after 10 min of low-current anodic dissolution at 0.95 V is given in Figure 8B. It is interesting to note that, under the present conditions, dissolution occurred exclusively at the S_2 *multiatomic* step-edges. No changes were observed either at the terraces or at the *monatomic* S_1 or S'_2 edges, although pit formation along the eroded S_2 steps should not be overlooked.

The preferential dissolution at S_2 evidently arises from differences in the step-atom configurations at S_1 and S_2. Such variation in step-atom arrangement can be discerned readily from the schematic drawing in Figure 9 of a stepped-Pd(100) surface with atoms at S_1 and S_2 exposed. The atomic architecture of the S_1 step, along the {110} direction, is the same as that of the (111) plane, indicated by the triangle; the atomic configuration at the S_2 step, parallel to the {100} direction, is identical with that on the (110) surface, shown by the rectangle. As indicated by the voltammetric data in Figure 3, at 0.95 V, detectable corrosion already takes place at Pd(110)−I but not at Pd(111)−I. Dissolution at the S_2 step, but not at the S_1 edge, is therefore not surprising. That the dissolved S_2-step atoms leave shallow pits in their wake may be due to the unique reactivity of the Pd(110)−I surface (vide infra). The stability of the S'_2 step along the {100} atomic row is almost certain because, at a monatomic height, this edge remains quite different from an ideal (110) plane.

Dissolution at 1.05 V. At this potential, the Pd(111)−I surface is no longer inert toward anodic dissolution (cf., Figure 3); consequently, when the potential is increased to 1.05 V, dissolution at the S_1 step may be anticipated. However, reaction at S_1 would still be at a comparatively negligible rate, since the overpotential for dissolution at S_2 has also been increased. Such expectations are borne out by the STM images in Figure 10 obtained after 5, 6, and 7 min at 1.05 V: only rectangular terraces with steps along the {100} edge and its orthogonal direction are recognizable.

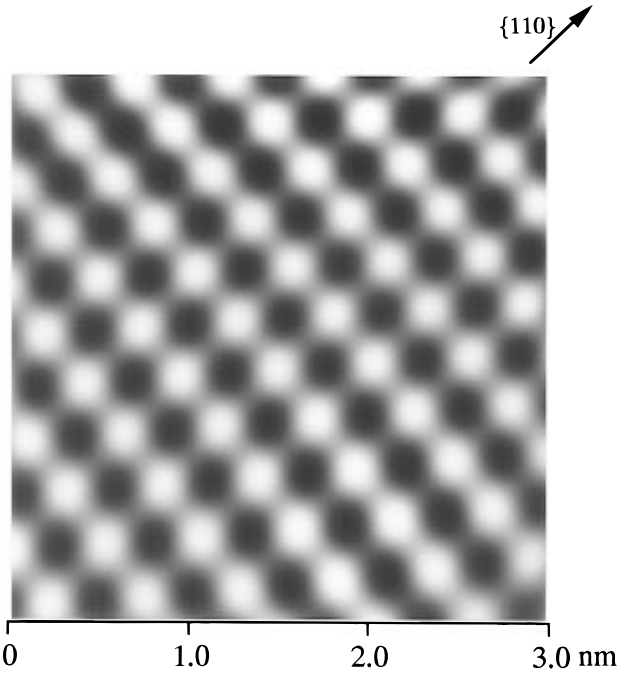

Figure 7. High-resolution STM image of Pd(100)-*c*(2 × 2)-I at 0.9 V in 0.05 M H_2SO_4. The potential of the tip was 0.8 V; the tunneling current was 1 nA.

It is first important to realize that, in contrast to the disorder that ensues from etching at 0.95 V (cf., Figure 8B), dissolution at 1.05 V resulted in an atomically flat surface topography. All steps were now only monatomic in height; that is, anodic dissolution at the higher potential led to diminution of the multiatom-high S_2 step-edges. This dissolution-generated disorder-to-order transformation is reminiscent of electrochemical "digital etching", in which well-ordered iodine adlattices were restored from extensively roughened (ion-bombarded) Pd(100) surfaces by adsorbate-catalyzed dissolution of the disordered layers.[21]

Closer inspection of the STM images in Figure 10 reveals that dissolution transpired only at step-edges; corrosion, via pit formation, was not observed at the terraces *(T)*. More significantly, it can be recognized that dissolution occurred anisotropically. For example, the "narrowing" (and subsequent disappearance) of the T_1, T_2, and T_3 terraces developed almost entirely along the [001]-directed step, with only minimal "narrowing" (if at all) in the direction perpendicular to it. Anisotropic dissolution has been reported earlier for sulfur-modified Ni(100) in acid sulfate solutions[22] and appears to be also operative in the corrosion of Cu(100) in Cl^- media.[23]

The absence of pit corrosion at the terraces and the selective dissolution at and the continuous retraction of the step-edges provide evidence that at 1.05 V the corrosion of Pd(100)−I proceeds via a layer-by-layer mechanism. In this regard, Pd(100)-*c*(2 × 2)-I behaves similarly to Pd(111)-($\sqrt{3} \times \sqrt{3}$)*R*30°-I.

The present case of anisotropic dissolution may be understood in terms of the schematic model in Figure 11 that depicts an I-pretreated Pd(100) surface with monatomic step-edges. From simple bond-counting considerations,[22] it can be argued that the Pd atoms A and B in the upper-left corner of the top terrace are the most reactive toward anodic dissolution. Removal of atom A (as in the case of dissolution along the {100}-directed step-edge) easily permits the iodine atom to slide down from a 4-fold site at the upper terrace onto another hollow site (H) at the lower terrace. On the other hand, iodine descent onto site

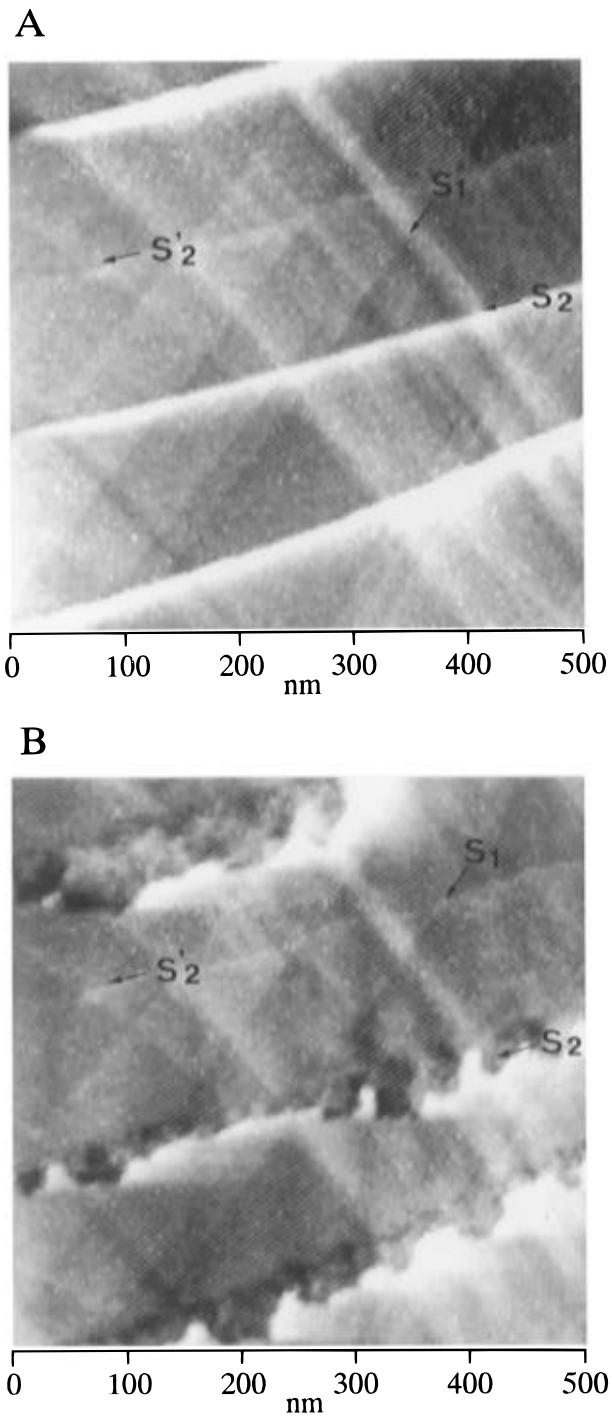

Figure 8. Wide-area STM images of Pd(100)-$c(2 \times 2)$-I at (A) 0.9 V and (B) after 10 min of corrosion at 0.95 V in 0.05 M H_2SO_4. S_1 marks the step that runs parallel to the {110} direction; S'_2 identifies a monatomic edge and S_2 a multiatomic step-edge aligned along the {100} direction. The potential of the tip was 0.9 V; the tunneling current was 1 nA.

H cannot be accomplished upon removal of atom B (dissolution along the orthogonal {010} direction) because of steric hindrance by atom A. The ease by which iodine diffuses from a high-symmetry site from the upper to lower terrace has been suggested as the major driving force in anisotropic dissolution.[22]

(iii) Pd(110)−I. LEED studies with an oriented bulk Pd(110) single crystal indicated low-background, discrete spots for both the clean and I-coated surfaces.[10] At least two structures were found for the Pd(110)−I surface: (i) Pd(110)-pseudohexagonal-I, which is generated spontaneously from open-circuit exposures to aqueous KI and (ii) Pd(110)-$c(2 \times 2)$-I, obtained either indirectly by heating the pseudohexagonal structure to 750 K

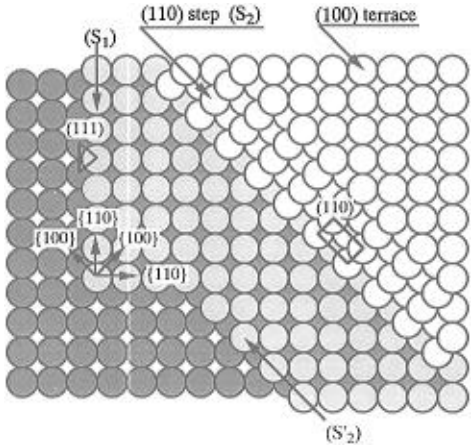

Figure 9. Schematic representation of a Pd(100) surface that contains steps oriented along the {100} and {110} directions. The atomic arrangements at these two steps are represented by the triangle [(111) plane)] and rectangle [(110) plane].

or directly by adsorption at potentials negative of the double-layer region. In this work, we surmise the existence of a pseudohexagonal adlayer, since iodine pretreatment was carried out in the absence of potential control.

In contrast to the other two low-index planes, wide terraces were not encountered with the I-free Pd(110)-(1×1) surface, despite meticulous metallographic polishing and high-temperature annealing. Wide-area STM images for the iodine-coated Pd(110) surface are shown in Figure 12; Figure 12A was obtained prior to anodic dissolution, while parts B−D of Figure 12 were acquired at preselected intervals after dissolution at 1.0 V. Wide terraces were likewise absent from the predissolution image (Figure 12A). Instead, corrugation along the {100} direction, one atomic layer in height and ca. 16 nm in width, was observed. The existence of a handful of randomly located pits, a few nanometers in diameter and up to three atomic layers in depth, can also be recognized.

Five minutes into the dissolution reaction, the population of pits, now several nanometers in diameter and up to 2 nm in depth, increased significantly (Figure 12B). Dramatic changes in the STM image resulted after extended dissolution (parts C and D of Figure 12). The more obvious ones are as follows. (i) The pits have become considerably larger with shapes that have been altered from circular to rectangular with edges that run parallel to the {110} and {100} directions. (ii) The rectangular terraces are invariably elongated toward the {100} direction. (iii) Rectangular pits have formed at the bottom of the rectangular pits. (v) The surface has become markedly roughened.

The evolution of the STM images on going from parts A to D of Figure 12, in particular the preferential elongation of the rectangular pits, is diagnostic of anisotropic dissolution. The formation of rectangular pits brought about by the dissolution process may be rationalized in terms of the schematic model presented in Figure 13 of a Pd(110) surface that contains a rectangular pit two atomic layers in depth. It can be seen from the model that the step-edge along the {110} direction is constituted by the (111) plane (triangle), whereas the step-edge in the {100} direction consists of the (100) plane (rectangle). Rectangular pits would be formed if dissolution occurred preferentially along *either* the {100} or {110} directions; isotropic corrosion would obviously result in square-shaped pits. The observation that the rectangular pits are elongated along the {100} direction suggests that the (111) step is preferentially (albeit slightly) corroded over the (100) edge. Such preferential dissolution is not inconsistent with the current−potential data

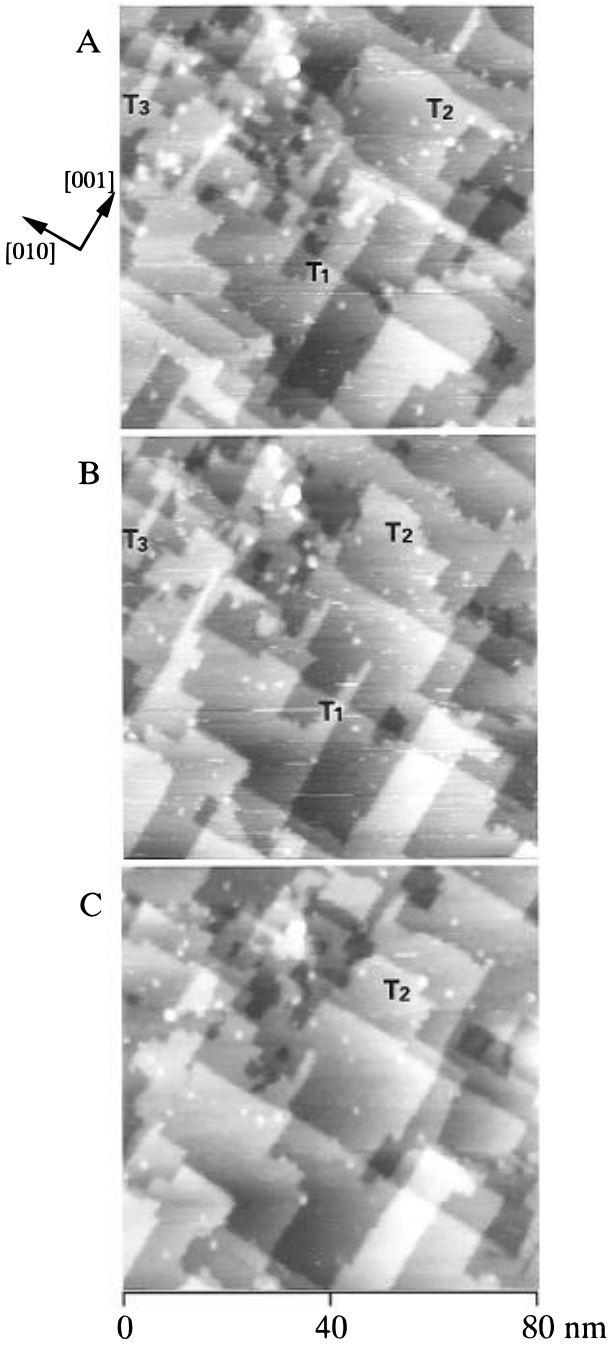

Figure 10. Medium-resolution STM images of Pd(100)-$c(2 \times 2)$-I obtained after (A) 5, (B) 6, and (C) 7 min of dissolution at 1.1 V in 0.05 M H_2SO_4. The letter T designates a terrace. The potential of the tip was 0.9 V; the tunneling current was 1 nA.

in Figure 3, which show that the onset of Pd(100)−I corrosion is at a potential (slightly) more positive than that of Pd(111)−I dissolution.

The propagation of pit corrosion on the upper terrace and inside the rectangular pits leads to progressive deterioration of the Pd(110)−I surface, a result that was initially indicated by the LEED data.[12] The formation of these pits is simply due to the dissolution of more active Pd atoms on the Pd(110) terrace-plane. In view of the aggressive reactivity of the Pd(110)−I surface relative to Pd(111)−I and Pd(100)−I (Figure 3), it may just be that pit corrosion on Pd(110)−I terraces cannot be completely eliminated.

Acknowledgment. This work was supported by Ministry of Education, Science and Culture and the ERATO−Itaya Electrochemiscopy Project, JRDC. M.P.S. acknowledges the Robert A. Welch Foundation and the Energy Resources Program of Texas A&M University.

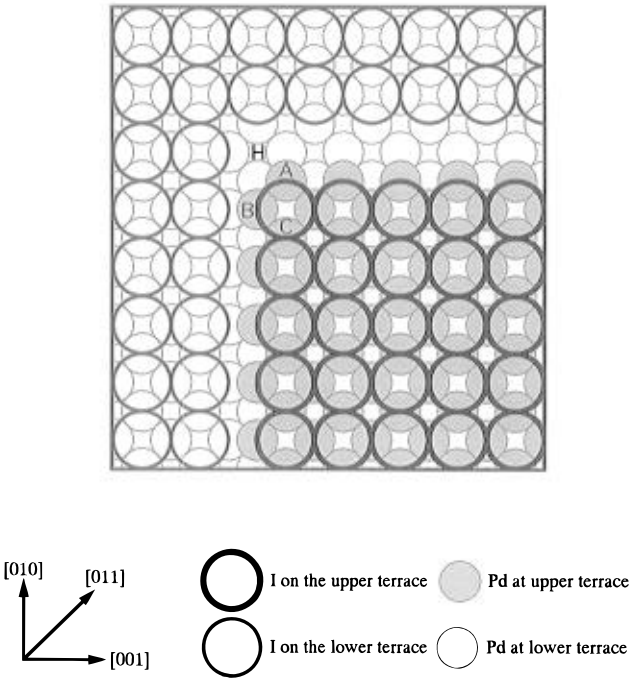

Figure 11. Schematic model of a stepped Pd(100)−I surface to illustrate anisotropic dissolution.

References and Notes

(1) (a) Somorjai, G. A. *Surface Chemistry and Catalysis*: Wiley-Interscience: New York, 1994. (b) Ertl, G.; Kuppers, J. *Low Energy Electrons and Surface Chemistry*; VCH Publishers: New York, 1985. (c) Woodruff, D. P.; Delchar, T. A. *Modern Techniques of Surface Science*, Cambridge University Press: New York, 1986.

(2) (a) Hubbard, A. T. *Acc. Chem. Res*. **1980**, *13*, 177. (b) Ross, P. N. In *Chemistry and Physics of Solid Surfaces*; Vanselow, R., Howe, R., Eds.; Springer-Verlag: New York, 1982. (c) Yeager, E.; Homa, A.; Cahan, B. D.; Scherson, D. *J. Vac. Sci. Technol*. **1982**, *20*, 628. (d) Kolb, D. M. *Z. Phys. Chem. Neue Folge*. **1987**, *154*, 179. (e) Soriaga, M. P. *Prog. Surf. Sci*. **1992**, *39*, 325.

(3) (a) Bard, A. J.; Abruña, H. D.; Chidsey, C. E.; Faulkner, L. R.; Feldberg, S. W.; Itaya, K.; Melroy, O.; Murray, R. W.; Porter, M. D.; Soriaga, M. P.; White, H. S. *J. Phys. Chem*. **1993**, *97*, 7147. (b) *Electrochemical Interfaces: Modern Techniques for In-Situ Surface Characterization*; Abruña, H., Ed.; VCH: New York, 1991.

(4) (a) Sonnenfield, R.; Hansma, P. K. *Science* **1986**, *232*, 211. (b) Dovek, M. M.; Heben, M. J.; Lewis, N. S.; Penner, R. M.; Quate, C. F. In *Electrochemical Surface Science*; Soriaga, M. P., Ed.; American Chemical Society: Washington, DC, 1988. (c) Itaya, K. In *The Handbook of Surface Imaging and Visualizatio*nl; Hubbard, A. T., Ed.; CRC Press: Boca Raton, FL, 1995.

(5) (a) Cataldi, T. R. I.; Blackham, I. G.; Briggs, G. A. D.; Pethica, J. B.; Hill, H. A. O. *J. Electroanal. Chem*. **1990**, *290*, 1. (b) Christensen, P. A. *Chem. Soc. Rev*. **1992**, 197. (c) Siegenthaler, K. In *Scanning Tunneling Microscopy II*; Wiesendanger, R., Güntherodt, J., Eds., Springer-Verlag Press: New York, 1992.

(6) (a) Schardt, B. C.; Yau, S.-L.; Rinaldi, F. *Science* **1989**, *243*, 1050. (b) Yau, S.-L.; Chang, S. C.; Schardt, B. C.; Weaver, M. J. *J. Am. Chem. Soc*. **1991**, *113*, 6049. (c) Sashikata, K.; Furuya, N.; Itaya, K. *J. Vac. Sci. Technol*. **1990**, *A8*, 515. (d) Magnussen, O. M.; Hotlos, J.; Nichols, R. J.; Kolb, D. M.; Behm, R. J. *Phys. Rev. Lett*. **1990**, *64*, 2929. (e) Itaya, K.; Sugawara, R.; Morita, Y.; Tokumoto, H. *Appl. Phys. Lett*. **1992**, *60*, 2535. (f) Carlsson, P.; Holmstrom, B.; Kita, H.; Uosaki, K. *J. Electroanal. Chem*. **1990**, *283*, 425. (g) Suggs, D. W.; Bard, A. J. *J. Am. Chem. Soc*. **1994**, *116*, 10725. (h) Lei, Q. P.; Stickney, J. L. *Mater. Res. Soc. Symp. Proc*. **1992**, *237*, 335. (i) Kunitake, M.; Batina, N.; Itaya, K. *Langmuir* **1995**, *11*, 2337.

(7) (a) Yamada, T.; Batina, N.; Itaya, K. *J. Phys. Chem*. **1995**, *99*, 8817. (b) Batina, N.; Yamada, T.; Itaya, K. *Langmuir* **1995**, *11*, 4568.

(8) Soriaga, M. P.; Schimpf, J. A.; Abreu, J. B.; Carrasquillo, A.; Temesghen, W.; Barriga, R. J.; Jeng, J.-J.; Sashikata, K.; Itaya, K. *Surf. Sci*. **1995**, *335*, 273.

(9) McBride, J. R.; Soriaga, M. P. *J. Electroanal. Chem*. **1991**, *303*, 255.

(10) Schimpf, J. A.; McBride, J. R.; Soriaga, M. P. *J. Phys. Chem*. **1993**, *97*, 10518.

(11) Schimpf, J. A.; Abreu, J. B.; Soriaga, M. P. *Langmuir* **1993**, *9*, 3331.

(12) Temesghen, W. F.; Abreu, J. B.; Lafferty, E. A.; Barriga, R. J.; Soriaga, M. P. *Surf. Sci*., submitted.

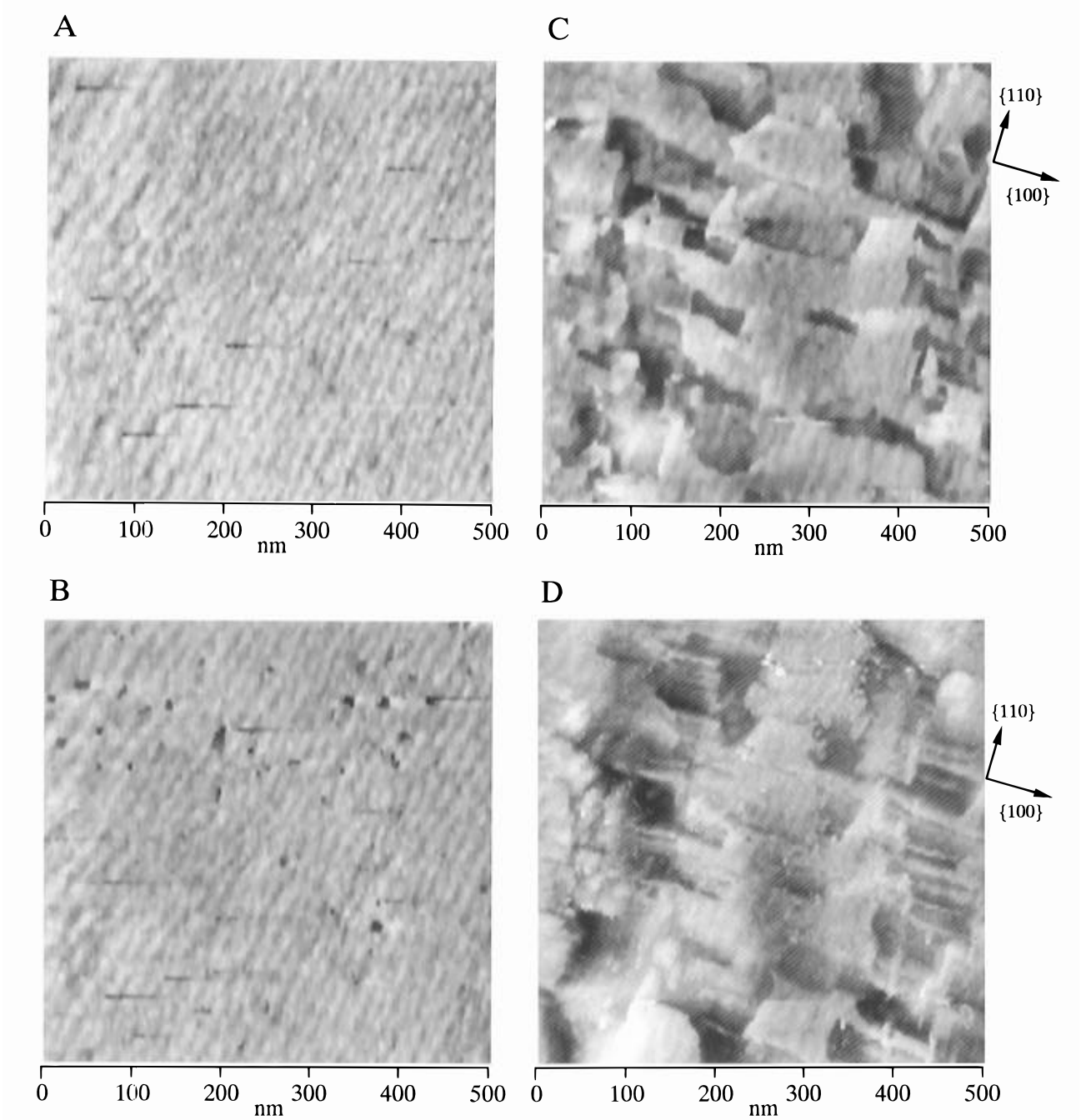

Figure 12. Wide-area STM images of Pd(110)−I: (A) prior to, (B) at the start of, (C) after 4 min, and (D) after 10 min of dissolution at 1.1 V in 0.05 M H_2SO_4. The potential of the tip was 0.9 V; the tunneling current was 1 nA.

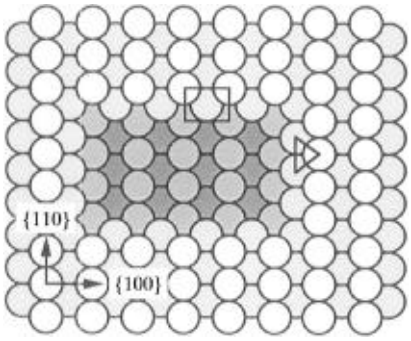

Figure 13. Schematic representation of a Pd(110) surface that contains a rectangular pit with steps that run parallel to the {100} and {110} directions. The atomic arrangements at these two steps are represented by the triangle [(111) plane)] and rectangle [(100) plane].

(13) Clavilier, J. *J. Electroanal. Chem.* **1980**, *107*, 211.
(14) Honbo, H.; Sugawara, S.; Itaya, K. *Anal. Chem.* **1990**, *62*, 2424.
(15) (a) Clavilier, J.; El Achi, K.; Rodes, A. *Chem. Phys.* **1990**, *141*, 1. (b) Furuya, N.; Koide, S. *Surf. Sci.* **1989**, *220*, 18. (c) Kozlowska, H. A.; Conway, B. E.; Hamelin, A.; Stoicoviciu, L. *J. Electroanal. Chem.* **1987**, *228*, 429. (d) Hourani, M.; Wasberg, M.; Rhee, C. K.; Wieckowski, A. *Croat. Chem. Acta* **1990**, *63*, 373. (e) Obretenov, W.; Bostanov, V.; Budevski, E. *J. Electroanal. Chem.* **1984**, *170*, 51. (f) Schott, J. H.; White, H. S. *J. Phys. Chem.* **1994**, *98*, 291. (g) Yau, S.-L.; Fan, F.-R.; Moffat, T. P.; Bard, A. J. *J. Phys. Chem.* **1994**, *98*, 5493.
(16) Chierchie, T.; Mayer, C.; Lorenz, W. J. *J. Electroanal. Chem.* **1982**, *135*, 211.
(17) (a) Somorjai, G. A. *Chemistry in Two Dimensions: Surfaces*; Cornell University Press: Ithaca, NY, 1981. (b) *The Nature of the Surface Chemical Bond*; Rhodin, T. H., Ertl, G. Eds.; North-Holland Publishing: New York, 1979.
(18) Wagner, F. T.; Ross, P. N. *Appl. Surf. Sci.* **1985**, *24*, 87.
(19) Conway, B. E.; Barnett, B.; Angerstein-Kozlowska, H.; Tilak, B. V. *J. Chem. Phys.* **1990**, *93*, 8361.
(20) Angerstein-Kozlowska, H.; Conway, B. E.; Hamelin, A.; Stoicoviciu, L. *J. Electroanal. Chem.* **1987**, *228*, 429.
(21) Schimpf, J. A.; Carrasquillo, A.; Soriaga, M. P. *Electrochim. Acta* **1995**, *40*, 1203.
(22) Ando, S.; Suzuki, T.; Itaya, K. *J. Electroanal. Chem.* **1996**, *412*, 139.
(23) Suggs, D. W.; Bard, A. J. *J. Phys. Chem.* **1995**, *99*, 8349.

JP9620532